Neutral-current supernova-neutrino cross sections for ^{204,206,208}Pb calculated by Skyrme quasiparticle random-phase approximation

W. Almosly,[1] B. G. Carlsson,[2] J. Suhonen,[1] and E. Ydrefors[3]
[1]*Department of Physics, University of Jyvaskyla, P.O. Box 35, FI-40014, Finland*
[2]*Division of Mathematical Physics, LTH, Lund University, P.O. Box 118, S-22100 Lund, Sweden*
[3]*Instituto Tecnológico de Aeronáutica, DCTA, 12228-900, São José dos Campos, SP, Brazil*

(Received 23 January 2019; revised manuscript received 12 March 2019; published 1 May 2019)

The present work constitutes a detailed study of neutral-current (NC) supernova-neutrino scattering off the stable even-even lead isotopes ^{204,206,208}Pb. This is a continuation of our previous work [Almosly *et al.*, Phys. Rev. C. **94**, 044614 (2016)] where we investigated charged-current processes on the same nuclei. As in the previous work, we have adopted the quasiparticle random-phase approximation (QRPA) as the theory framework and use three different Skyrme interactions to build the involved nuclear wave functions. We test the Skyrme forces by computing the location of the lowest-order isovector spin-multipole giant resonances and comparing with earlier calculations. We have computed the NC cross sections for (anti)neutrino energies up to 100 MeV and estimated the nuclear responses to supernova (anti)neutrinos by folding the obtained cross sections by suitably parametrized Fermi-Dirac distributions of energies of the incoming (anti)neutrinos. We compare our results with results of earlier studies in the case of ^{208}Pb, which is the only lead isotope where earlier calculations are available.

DOI: 10.1103/PhysRevC.99.055801

I. INTRODUCTION

Neutrino-nucleus interactions are crucial in exploring the structure of the weak hadronic current and the unknown neutrino properties. Neutrino reactions with nuclei contribute to the studies of the underlying structure of nuclear weak processes [1]. The cross sections of the neutral-current neutrino-nucleus scattering can, in combination with charged-current reactions, be useful to detect and distinguish between neutrinos of different flavors. Furthermore, the cross sections of the charged-current reactions can be used, e.g., in the studies of neutrinoless double-β decay. This process can be used to determine the absolute mass of the neutrino and possibly the phases in the mixing matrix. In addition, observation of this process would imply that neutrinos are Majorana particles [2–5].

Knowledge of neutrino-nucleus scattering is also essential for many applications in astrophysics, in particular in the investigation of supernova mechanisms [6]. Nuclear responses to supernova neutrinos constitute important inputs in supernova simulations [7]. Moreover, the cross sections for the scattering off of certain nuclei, at energies relevant for supernova neutrinos, are of interest for nuclear astrophysics in tracing the various processes that lead to stellar nucleosynthesis [7]. Due to various experimental difficulties, only theoretical estimation of cross sections for different target nuclei is available in order to provide the needed input in the aforementioned and other applications of astrophysics as well as neutrino physics.

In addition to supernova discoveries, neutrino-nucleus interactions are important for dark-matter detection experiments. As the sensitivity of future dark-matter detectors increases, in particular the experiments based on xenon isotopes, the solar, atmospheric, and supernova neutrinos can turn into an unwanted background, the so-called neutrino floor [8]. Thus, it will be important to quantify the cross sections of such neutrinos. Therefore neutrino-nucleus calculations for targets of future interest are relevant to neutrino-floor studies (see, for example, [9]).

Theoretical estimates of neutrino-nucleus cross sections can be an important key to interpreting the neutrino signals measured by Earth-bound detectors. Neutrinos interact weakly with matter and can be detected by using neutral-current and charged-current neutrino-nucleus reactions on massive targets. Several neutrino-detector facilities are being established and planned around the world for the detection of the core-collapse-supernova-associated neutrinos [10]. Current and future detectors involve a variety of target materials such as carbon, oxygen, argon, and lead nuclei. The lead nuclei, the target nuclei in the present work, are in use at the Helium and Lead Observatory (HALO) experiment [11] running at SNOLAB, the Sudbury Neutrino Observatory in Canada. The HALO experiment is aimed to detect electron neutrinos and antineutrinos through the charged-current reactions and all neutrino flavors through the neutral-current reactions.

The purpose of this work is to extend our previous work [12] on charged-current supernova-neutrino scattering off the stable even-even lead isotopes to study the neutral-current reactions. To our knowledge, this is the first study of neutral-current reaction on the ^{204,206}Pb isotopes. In the present work the required wave functions for the ground state and all possible final states are constructed in the context of the quasiparticle random-phase approximation (QRPA). The two-body interaction is taken to be of the Skyrme type

where the Skyrme SkM*, SkX, and SLy4 parametrizations are investigated. These interactions are used to construct the nuclear quasiparticle mean field and the QRPA excitations in a consistent way. The formalism employed for the scattering calculations is based on the Donnelly-Walecka method for the treatment of semileptonic processes in nuclei [13]. Estimates of the response of lead nuclei to supernova neutrinos are computed by folding the obtained total cross sections with two-parameter Fermi-Dirac distributions.

The present article is organized as follows: First, in Sec. II, the theoretical framework is briefly outlined. The nuclear-structure ingredients are introduced first and then the basic formalism of the neutral-current neutrino-nucleus scattering is briefly summarized. Then, in Sec. III, the obtained results are presented and discussed. Finally, in Sec. IV conclusions of the gained results are drawn.

II. THEORY

A. Nuclear-structure formalism

The ground states of the considered nuclei are obtained through the Hartree-Fock-Bogoliubov (HFB) approach where the nuclear effective interaction is approximated with density-dependent Skyrme interactions. In this way the expression for energy takes the form of a density functional [14].

The parameters of the nuclear density functionals are typically fitted to describe a collection of experimental data such as binding energies and radii. Three such parametrizations are investigated. The SkX parametrization has been tuned with special focus on describing nuclear energy spectra [15]. The SkM* parametrization is tuned to describe collective excitations and deformation properties [16,17], and the SLy4 interaction has been constructed with specific attention to neutron-rich nuclei [18].

The nucleon pairing is modeled by a Gaussian-type pairing interaction in a separable form [19], with different strengths for each of the considered Skyrme functionals [20]. The nuclear excitations are calculated using the quasiparticle random-phase approximation employing the same functional as for the ground states [20]. For the spherical nuclei considered here, the excitations can be sorted into groups with specific angular momentum J and parity π so that the QRPA can be separately solved for each multipolarity J^π. For each J^π combination the excitations are extracted by fully diagonalizing the QRPA matrix, keeping all states up to a maximum main oscillator shell $N_{\max} = 15$ in the spherical oscillator basis. The HFB and QRPA equations are solved using an updated version [20] of the code HOSPHE [21].

B. Cross-section formalism

This section summarizes briefly the formalism for the neutral-current (NC) supernova neutrino-nucleus scattering. A detailed treatment can be found in [22].

The neutral-current reaction proceeds via the exchange of a neutral Z^0 boson. The transferred four-momentum fulfills the condition $Q^2 = -q_\mu q^\mu \ll M_Z^2$ where M_Z is the mass of the Z^0 boson.

The corresponding matrix element of the effective Hamiltonian in this case is written in the form

$$\langle f|H_{\text{eff}}|i\rangle = \frac{G_{\text{F}}}{\sqrt{2}} \int d^3\mathbf{r} l_\mu e^{-i\mathbf{q}\cdot\mathbf{r}} \langle f|\mathcal{J}^\mu(\mathbf{r})|i\rangle, \tag{1}$$

where $\mathcal{J}^\mu(\mathbf{r})$ denotes the hadron current and l_μ is the lepton matrix element: $l_\mu = e^{i\mathbf{q}\cdot\mathbf{r}}\langle f|j_\mu(r)|i\rangle$.

The double-differential cross section for the (anti)neutrino scattering from the initial state $|J_i\rangle$ to a finial state $|J_f\rangle$ is given by

$$\left[\frac{d^2\sigma_{i\to f}}{d\Omega dE_{\text{exc}}}\right]_{\nu_e/\bar{\nu}_e} = \frac{G_{\text{F}}^2|\mathbf{k}'|E_{\mathbf{k}'}}{\pi(2J_i+1)}\left(\sum_{J\geqslant 0}\sigma_{\text{CL}}^J + \sum_{J\geqslant 1}\sigma_{\text{T}}^J\right), \tag{2}$$

where $\mathbf{k}'$ and $E_{\mathbf{k}'}$ are the three-momentum and the energy of the outgoing (anti)neutrino. The Coulomb-longitudinal component σ_{CL}^J and the transverse component σ_{T}^J are defined as

$$\begin{aligned}\sigma_{\text{CL}}^J =& (1+\cos\theta)|(J_f\|\mathcal{M}_J(q)\|J_i)|^2 \\ &+ \left(1+\cos\theta - 2\frac{E_{\mathbf{k}}E_{\mathbf{k}'}}{q^2}\sin^2\theta\right)|(J_f\|\mathcal{L}_J(q)\|J_i)|^2 \\ &+ \frac{E_{\mathbf{k}}-E_{\mathbf{k}'}}{q}(1+\cos\theta) \\ &\times 2\text{Re}[(J_f\|\mathcal{L}_J(q)\|J_i)(J_f\|\mathcal{M}_J(q)\|J_i)^*],\end{aligned} \tag{3}$$

and

$$\begin{aligned}\sigma_{\text{T}}^J =& \left(1-\cos\theta+\frac{E_{\mathbf{k}}E_{\mathbf{k}'}}{q^2}\sin^2\theta\right) \\ &\times\left[|(J_f\|\mathcal{T}_J^{\text{mag}}(q)\|J_i)|^2 + |(J_f\|\mathcal{T}_J^{\text{el}}(q)\|J_i)|^2\right] \\ &\mp \frac{(E_{\mathbf{k}}+E_{\mathbf{k}'})}{q}(1-\cos\theta) \\ &\times 2\text{Re}\left[(J_f\|\mathcal{T}_J^{\text{mag}}(q)\|J_i)(J_f\|\mathcal{T}_J^{\text{el}}(q)\|J_i)^*\right].\end{aligned} \tag{4}$$

Here the minus sign refers to neutrino and the plus sign to antineutrino scattering, θ is the lepton scattering angle, $E_{\mathbf{k}}$ is the energy of the incoming (anti)neutrino, and q is the magnitude of the three-momentum transfer

$$q = |\mathbf{q}| = \sqrt{(E_{\mathbf{k}}-E_{\mathbf{k}'})^2 + 2E_{\mathbf{k}}E_{\mathbf{k}'}(1-\cos\theta)}. \tag{5}$$

The multipole operators $\mathcal{T}_{JM} = \mathcal{M}_{JM}, \mathcal{L}_{JM}, \mathcal{T}_{JM}^{\text{el}}$, and $\mathcal{T}_{JM}^{\text{mag}}$ are defined in [23]. These multipole operators contain the nucleon form factors $F_{1,2}^{\text{V}}(Q^2)$ (vector), $F^{\text{A}}(Q^2)$ (axial-vector), and $F^{\text{P}}(Q^2)$ (pseudoscalar), which, in turn, depend on the four-momentum transfer. These form factors take into account the finite-size effects of the nucleons. The adopted form factors are presented in [22]. The axial form factors depend on the axial-vector coupling strength g_{A}. We adopt the dipole form of this strength [22] for finite momentum transfer $q > 0$ and adopt the (moderately) quenched value $g_{\text{A}}(0) = 1.0$ at the zero momentum transfer. We use the same quenched value for all multipole states J^π in the calculations since there is evidence that quenching at $q = 0$ occurs also for higher multipoles [5,24,25].

III. RESULTS

We perform in this work a detailed study of the NC nuclear responses to supernova neutrinos and antineutrinos for the stable even-even lead isotopes ^{204,206,208}Pb. We follow the logic of our previous study of the charged-current (anti)neutrino scattering off the same lead isotopes [12].

We adopted QRPA for the nuclear-structure framework. For the two-body interaction we have selected three recently developed Skyrme forces, namely, SkM*, SkX, and SLy4 [26]. The code HOSPHE [21] was used to calculate the HFB ground state and the QRPA excitations. We adopted from [20] the two values for the parameters G_n (neutrons) and G_p (protons) of the separable Gaussian pairing. The pairing strengths in [20] are related to the isovector strength G_1 only. As our QRPA calculations depend on both the isoscalar and isovector pairing strengths G_0 and G_1, we adopted here the prescription $G_0 = G_1$, used in our earlier works [12,27]. In other words, we perform two QRPA calculations: in the first one we choose for the pairing strengths $G_0 = G_1 = G_n$ and in the second model we choose $G_0 = G_1 = G_p$ (see Table II of Ref. [20] for the numerical values of the pairing strengths).

A. $M1$ and isovector spin-multipole excitations in ^{208}Pb

First we examine the strength distributions of the magnetic dipole $M1$ operator in ^{208}Pb in Fig. 1, where the strength is given in units of the nuclear magneton squared. The corresponding giant resonance is important for the NC scattering. The available experimental data on the $M1$ strength are summarized in Ref. [28]. According to data the experimental strength concentrates mostly within the range 7.3–7.5 MeV which can be considered to constitute the $M1$ giant resonance. In the calculations the $M1$ strength is carried by one state, located at 7 MeV, in the case of the SkX interaction. The strength is split into two states at about 7.3 and 9.8 MeV for the SkM* interaction and at 7.6 and 9.7 MeV for the SLy4 interaction, and most of the strength concentrates in the higher-energy state. It can be concluded that the computed strength with the SkX force is at a slightly lower energy than the experimental one but qualitatively the experimental giant resonance is reproduced by the calculation. For the SkM* and SLy4 interactions the strength is concentrated at a higher energy than in the experiment by about 2 MeV. A similar pattern repeats itself for ^{204}Pb and ^{206}Pb: the relative strengths of the split peaks are the same as in the case of ^{208}Pb, the position of the main peak shifting some 0.1 MeV higher with every two units less of mass number. For the SkM* and SLy4 interactions the lower peak corresponds to the leading QRPA configuration proton-$0h_{11/2}$-proton-$0h_{9/2}$ and the higher peak to the leading configuration neutron-$0i_{13/2}$-neutron-$0i_{11/2}$. For the SkX interaction these two configurations have roughly equal amplitudes in the one main $M1$ peak. The same repeats for all three lead isotopes. These findings are in line with the results of [29] for ^{208}Pb using the SkM* interaction.

The excitation energies for the isovector spin-dipole ($L = 1$ and $J = 0^-, 1^-, 2^-$) and for the isovector spin-quadrupole ($L = 2$ and $J = 1^+, 2^+, 3^+$) giant resonances can be accessed in our calculations at the limit of zero momentum transfer, i.e. at $q = 0$. The computed excitation energies of these resonances are shown in Table I. These excitation energies are similar in our two QRPA descriptions, where either the pairing strength G_n or G_p has been used, and thus only one set of values is given in the table. The average excitation energies for the isovector spin-dipole and spin-quadrupole strengths can be compared with those calculated in Ref. [30] using a continuum HF-RPA framework and the Skyrme SIII

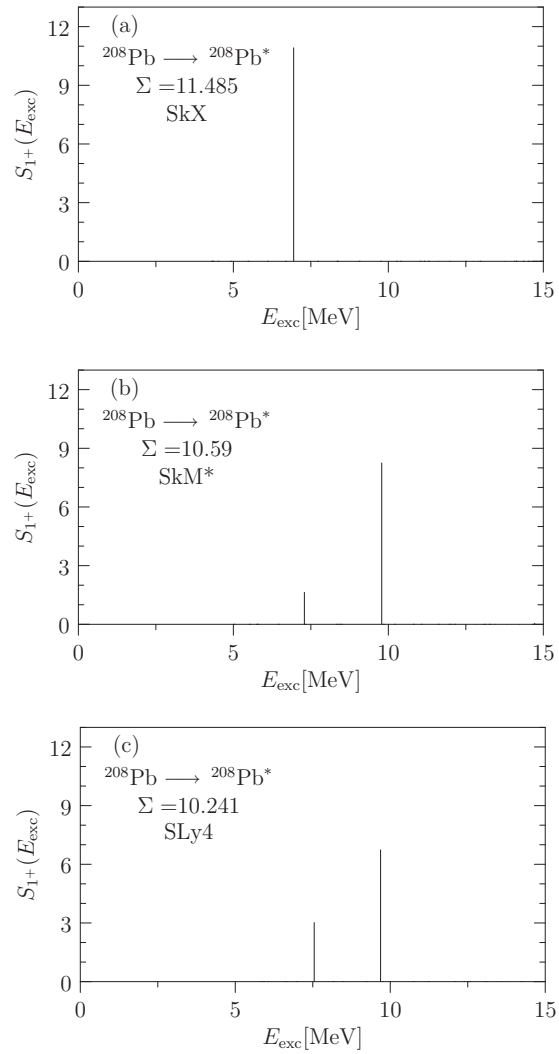

FIG. 1. Distribution of the $M1$ strength (in units of μ_N^2) in ^{208}Pb for the Skyrme interactions (a) SkX, (b) SkM*, and (c) SLy4.

TABLE I. Average energies for the transitions to J^π states with $L = 1, 2$ for ^{208}Pb. The energies are in MeV.

L	J^π	SkM*	SkX	SLy4	Ref. [30]
1	0^-	19.7	16.6	20.0	20.3
	1^-	16.4	14.1	17.0	16.9
	2^-	13.1	11.7	13.6	14.3
2	1^+	26.8	23.9	26.6	27.9
	2^+	22.1	20.0	22.7	23.9
	3^+	17.0	16.0	18.2	19.3

TABLE II. Total cross sections for the neutral-current neutrino scatterings in units of 10^{-42}cm^2. The exponents are given in parentheses. The values on the left correspond to the computation with pairing strength G_n and on the right with G_p. The total cross sections for ^{208}Pb are practically independent of the value of the pairing strength so that only one value is given.

	^{204}Pb			^{206}Pb		
$E_{\mathbf{k}}$ (MeV)	SkM*	SkX	SLy4	SkM*	SkX	SLy4
5.0	(3.75,7.01) (−2)	(2.25,3.48) (−2)	(3.14,5.27) (−2)	(3.81,7.22) (−2)	(2.39,3.73) (−2)	(3.35,6.25) (−2)
10.0	(6.76,9.01) (−1)	(1.67,1.79) (0)	(6.16,7.60) (−1)	(5.43,7.27) (−1)	(1.77,1.87) (0)	(5.62,7.2) (−1)
15.0	(6.65,7.30) (0)	(1.16,1.20) (1)	(6.57,7.00) (0)	(6.45,6.92) (0)	(1.22,1.25) (1)	(6.64,7.05) (0)
20.0	(2.23,2.34) (1)	(3.18,3.25) (1)	(2.12,2.21) (1)	(2.20,2.28) (1)	(3.33,3.38) (1)	(2.16,2.24) (1)
25.0	(4.98,5.18) (1)	(6.65,6.77) (1)	(4.68,4.83) (1)	(4.98,5.11) (1)	(6.93,7.02) (1)	(4.77,4.89) (1)
30.0	(9.42,9.71) (1)	(1.22,1.24) (2)	(8.80,9.01) (1)	(9.45,9.64) (1)	(1.27,1.28) (2)	(8.94,9.11)(1)
40.0	(2.55,2.60) (2)	(3.22,3.26) (2)	(2.38,2.42) (2)	(2.57,2.60) (2)	(3.32,3.35) (2)	(2.40,2.43) (2)
50.0	(5.48,5.55) (2)	(6.87,6.93) (2)	(5.12,5.19) (2)	(5.51,5.55) (2)	(7.04,7.08) (2)	(5.14,5.17) (2)
60.0	(1.01,1.02) (3)	(1.26,1.27) (3)	(9.38,9.50) (2)	(1.01,1.02) (3)	(1.29,1.29) (3)	(9.39,9.44) (2)
70.0	(1.64,1.66) (3)	(2.06,2.07) (3)	(1.53,1.56) (3)	(1.65,1.66) (3)	(2.10,2.11) (3)	(1.53,1.54) (3)
80.0	(2.46,2.47) (3)	(3.09,3.10) (3)	(2.28,2.30) (3)	(2.47,2.48) (3)	(3.14,3.15) (3)	(2.28,2.29) (3)
90.0	(3.47,3.54) (3)	(4.31,4.33) (3)	(3.16,3.18) (3)	(3.44,3.45) (3)	(4.38,4.39) (3)	(3.17,3.18) (3)
95.0	(3.95,3.97) (3)	(4.98,5.00) (3)	(3.64,3.67) (3)	(3.97,3.98) (3)	(5.06,5.07) (3)	(3.65,3.66) (3)

	^{208}Pb		
$E_{\mathbf{k}}$(MeV)	SkM*	SkX	SLy4
5.0	8.21 (−9)	4.16 (−5)	7.35 (−9)
10.0	2.22 (−1)	1.74 (0)	3.11 (−1)
15.0	5.81 (0)	1.24 (1)	6.22 (0)
20.0	2.10 (1)	3.39 (1)	2.11 (1)
25.0	4.87 (1)	7.10 (1)	4.74 (1)
30.0	9.37 (1)	1.30 (2)	8.94 (1)
40.0	2.57 (2)	3.40 (2)	2.41 (2)
50.0	5.52 (2)	7.20 (2)	5.15 (2)
60.0	1.01 (3)	1.31 (3)	9.41 (2)
70.0	1.66 (3)	2.14 (3)	1.53 (3)
80.0	2.48 (3)	3.19 (3)	2.29 (3)
90.0	3.45 (3)	4.45 (3)	3.18 (3)
95.0	3.99 (3)	5.14 (3)	3.66 (3)

interaction. Also these results are shown in Table I for easy comparison. A fair agreement can be seen in general. The SLy4 interaction shows the best agreement with [30]. The average excitation energies for the SkX force are shifted downward as compared to the computed energies of the other interactions. This qualitative pattern resembles the one discussed above for the $M1$ excitations: also there the SkX force predicted a lower energy of the $M1$ giant resonance than the other two Skyrme interactions. Since in the $M1$ case the SkX results agreed with the experimental data it could be that also for the spin-multipole resonances its prediction is the most reliable one. It is plausible that the good performance of the SkX interaction can be derived from the fact that is has been optimized to describe well the excitation energies in nuclei.

B. Total cross sections

The total cross sections were obtained by computing first the double-differential cross section of Eq. (2) and then by numerical integration over the scattering angle and subsequently summing over the discrete final states. Tables II and III provide the obtained results for neutrino scattering and antineutrino scattering, respectively. The chosen value of the pairing strength has a small effect on the total cross sections for the scattering off ^{204,206}Pb whereas both adopted pairing strengths give practically the same results for the scattering off ^{208}Pb.

Our total cross sections for neutrino scattering off ^{208}Pb are also presented in Fig. 2 and compared with the results of Refs. [31] and [32]. As can be seen from the figure, the SkX interaction gives larger cross sections compared to SkM* and SLy4. This can be explained by the low energy of the $M1$ resonance in the SkX calculation as compared to the other studied interactions (see Fig. 1). The cross sections of Ref. [31] are smaller than ours computed with the SkX interaction and a bit larger than those calculated by using the SkM* interaction. The cross sections predicted in Ref. [32] are close to our predicted cross sections with the SkX interaction. It is worth

TABLE III. Same as Table II, but for antineutrino scattering.

	^{204}Pb			^{206}Pb		
$E_{\mathbf{k}}$ (MeV)	SkM*	SkX	SLy4	SkM*	SkX	SLy4
5.0	(3.68,6.90) (−2)	(2.22,3.42) (−2)	(3.08,5.16) (−2)	(3.74,7.08) (−2)	(2.34,3.66) (−2)	(3.29,6.12) (−2)
10.0	(6.46,8.61) (−1)	(1.60,1.71) (0)	(5.89,7.26) (−1)	(5.17,6.93) (−1)	(1.70,1.80) (0)	(5.36,6.87) (−1)
15.0	(6.24,6.85) (0)	(1.09,1.12) (1)	(6.16,6.56) (0)	(6.05,6.49) (0)	(1.14,1.17) (1)	(6.22,6.61) (0)
20.0	(2.04,2.15) (1)	(2.91,2.98) (1)	(1.95,2.03) (1)	(2.02,2.10) (1)	(3.05,3.10) (1)	(1.98,2.05) (1)
25.0	(4.45,4.63) (1)	(5.93,6.04) (1)	(4.19,4.32) (1)	(4.44,4.56) (1)	(6.17,6.26) (1)	(4.26,4.37) (1)
30.0	(8.17,8.42) (1)	(1.05,1.07) (2)	(7.63,7.83) (1)	(8.18,8.34) (1)	(1.09,1.10) (2)	(7.74,7.89) (1)
40.0	(2.09,2.13) (2)	(2.61,2.64) (2)	(1.95,1.99) (2)	(2.09,2.12) (2)	(2.69,2.71) (2)	(1.96,1.98) (2)
50.0	(4.26,4.32) (2)	(5.28,5.32) (2)	(3.99,4.06) (2)	(4.26,4.29) (2)	(5.39,5.42) (2)	(3.98,4.02) (2)
60.0	(7.48,7.56) (2)	(9.22,9.28) (2)	(7.03,7.13) (2)	(7.48,7.52) (2)	(9.39,9.42) (2)	(6.99,7.03) (2)
70.0	(1.18,1.19) (3)	(1.45,1.45) (3)	(1.11,1.12) (3)	(1.18,1.18) (3)	(1.47,1.47) (3)	(1.10,1.11) (3)
80.0	(1.69,1.70) (3)	(2.08,2.09) (3)	(1.59,1.61) (3)	(1.69,1.70) (3)	(2.11,2.11) (3)	(1.58,1.59) (3)

	^{208}Pb		
$E_{\mathbf{k}}$ (MeV)	SkM*	SkX	SLy4
5.0	9.92 (−9)	3.72 (−5)	8.13 (−9)
10.0	2.09 (−1)	1.67 (0)	2.96 (−1)
15.0	5.46 (0)	1.16 (1)	5.83 (0)
20.0	1.93 (1)	3.11 (1)	1.94 (1)
25.0	4.35 (1)	6.32 (1)	4.22 (1)
30.0	8.09 (1)	1.12 (2)	7.72 (1)
40.0	2.08 (2)	2.75 (2)	1.96 (2)
50.0	4.25 (2)	5.49 (2)	3.97 (2)
60.0	7.47 (2)	9.54 (2)	6.97 (2)
70.0	1.18 (3)	1.49 (3)	1.10 (3)
80.0	1.70 (3)	2.14 (3)	1.58 (3)

mentioning that in Ref. [31] the RPA framework is adopted for the nuclear structure calculations and the single-particle energies are obtained from a Woods-Saxson potential. As a two-body interaction the zero-range Landau-Migdal force was used. The results of Ref. [32] are based on the RPA framework in the basis of Hartree-Fock states and using the SIII Skyrme interaction. Our calculations, in turn, are based on the QRPA with self-consistent mean field and two-body interactions stemming from more recent Skyrme forces.

The total cross sections for neutrino scattering off ^{208}Pb are also presented in Ref. [33] for two values of neutrino energy. The predicted cross section in Ref. [33] for neutrino energy 15 MeV is 0.199×10^{-40} cm^2 which is larger than our predicted interval produced by our adopted Skyrme

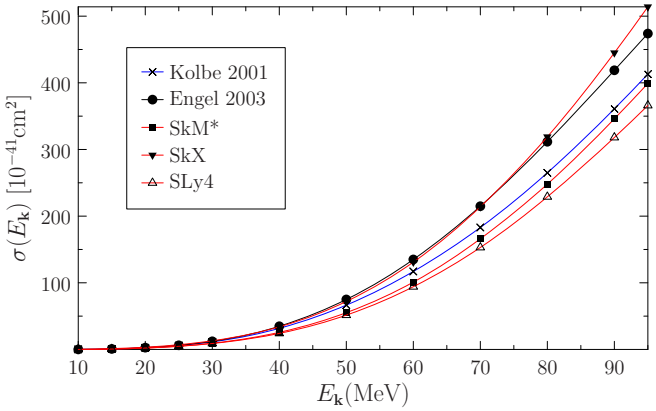

FIG. 2. Total cross sections as functions of the energy of the incoming neutrino for ^{208}Pb. Kolbe 2001 refers to [31] and Engel 2003 refers to [32].

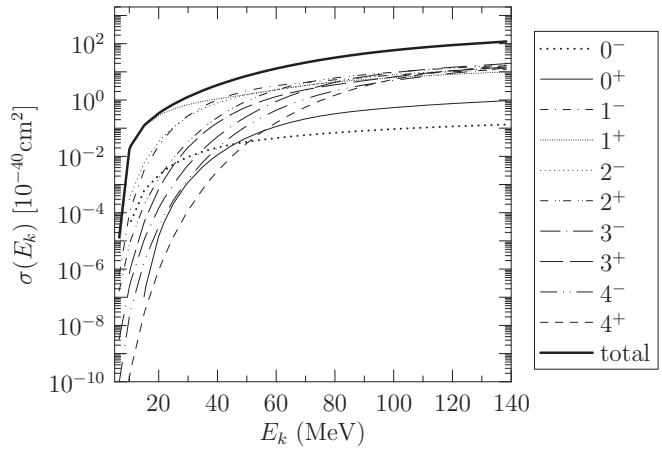

FIG. 3. Contributions from different multipole channels to the total cross section as functions of the energy of the incoming neutrino for the scattering off ^{208}Pb using the SkX interaction.

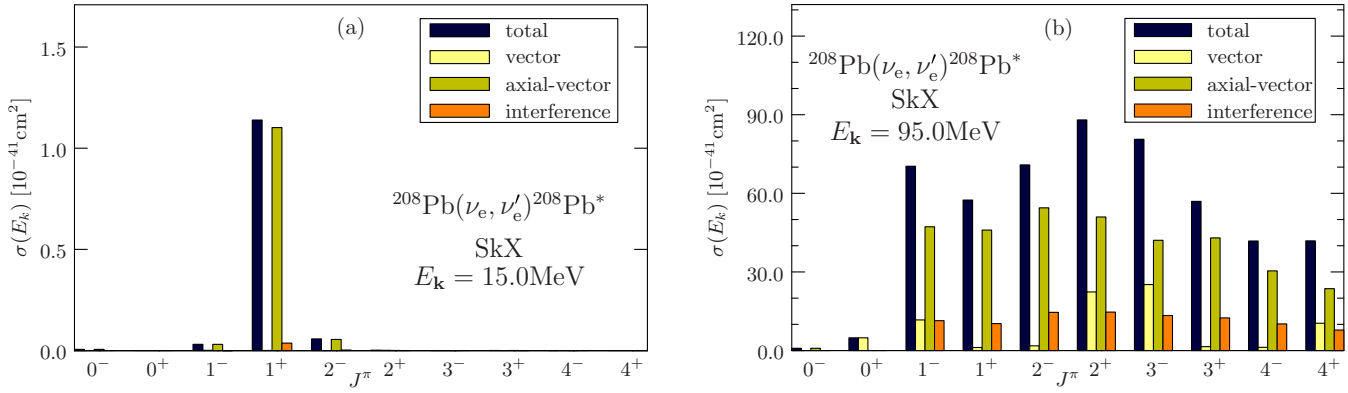

FIG. 4. Contributions of the various multipole channels to the cross sections of the neutrino scattering off ^{208}Pb for the neutrino energies (a) 15.0 and (b) 95.0 MeV. The interaction SkX has been used in the computations.

forces $(0.058–0.12) \times 10^{-40}$ cm^2 and it is also larger than the cross section 0.0798×10^{-40} cm^2 in Ref. [31] and 0.08×10^{-40} cm^2 in Ref. [32]. For neutrino energy 95 MeV the cross section 38.74×10^{-40} cm^2 of [33] falls inside our computed interval $(36.66–51.40) \times 10^{-40}$ cm^2 and is smaller than 41.3×10^{-40} cm^2 of Ref. [31] and 47.39×10^{-40} cm^2 of Ref. [32]. The nuclear structure of ^{208}Pb in Ref. [33] has been dealt with by a diagonalization of the δ-force interaction in the space of particle-hole excitations based on a single-particle basis containing 22 neutron and 29 proton harmonic-oscillator states.

More detailed information on the scattering cross sections can be obtained by studying the contributions from the different multipole channels. Therefore, we show in Fig. 3 the cross sections corresponding to the leading multipoles as functions of the energy of the impinging neutrino. The results displayed in the figure stem from calculations with the SkX interaction. Similar patterns can be observed for the other studied interactions. The figure shows that the largest contribution comes from the 1^+ multipole for neutrino energies $E_k \leqslant 40$ MeV. For energies $40 < E_k \leqslant 70$ MeV the 1^- transitions become important. Then comes the 2^+ and 3^- dominance for higher neutrino energies. In Fig. 4 we illustrate the main multipole contributions for neutrino energies 15 and 95 MeV. The contributions to each multipole from axial-vector, vector, and interference components are shown also in the figure. As can be seen in the figure, the 1^+ multipole with axial-vector character is the most significant for the neutrino energy 15 MeV while for the neutrino energy 95 MeV there are several contributing multipole channels. These results can be compared with those available in Ref. [33]. The 1^+ transitions in Ref. [33] have the most significant contribution at low neutrino energies which agrees with our results. In the high-energy region the excitations by the 1^+ multipole are still the most prominent ones in Ref. [33] whereas in our multipole decomposition higher multipoles begin to play a dominant role. This increase in the importance of the higher multipoles is consistent with the results obtained for the neutrino scattering off the Mo isotopes in Ref. [34].

C. Averaged cross sections

The averaged cross sections are obtained by folding the computed cross sections with an appropriate neutrino spectrum. The energy spectra of supernova neutrinos in this work are described by a two-parameter Fermi-Dirac distribution. The averaged cross sections then take the form

$$\langle \sigma_\nu \rangle = \frac{1}{F_2(\alpha_\nu) T_\nu^3} \int \frac{E_\nu^2 \sigma(E_\nu) dE_\nu}{1 + \exp(E_\nu/T_\nu - \alpha_\nu)}, \qquad (6)$$

where the parameters T_ν and α_ν represent the effective neutrino temperature and the pinching parameter, respectively. The constant $F_2(\alpha_\nu)$ normalizes the total neutrino flux to unity. The adopted values of the neutrino parameters for this work are displayed in Table IV. Our computed averaged cross sections are tabulated in Tables V and VI.

As expected, the averaged cross section increases with increasing neutrino temperature and decreasing pinching parameter. The SkX force gives the largest cross sections and the SLy4 force gives the smallest ones. This feature is in line with the earlier observations that 1^+ states are strongly populated by the neutrino scattering at low energies (see Fig. 4) and the $M1$ resonance (see Fig. 1) is responsible for the major contribution. Since SkX predicts the lowest energy of the

TABLE IV. Parameters α and T, and the average neutrino energies for two different supernova scenarios adopted from Ref. [35]. x denotes the nonelectron flavors, i.e., $x = \mu, \tau$.

	$(\alpha_{\nu_e}, T_{\nu_e}, \langle E_{\nu_e} \rangle)$	$(\alpha_{\bar{\nu}_e}, T_{\bar{\nu}_e}, \langle E_{\bar{\nu}_e} \rangle)$	$(\alpha_{\nu_x}, T_{\nu_x}, \langle E_{\nu_x} \rangle)$	$(\alpha_{\bar{\nu}_x}, T_{\bar{\nu}_x}, \langle E_{\bar{\nu}_x} \rangle)$
(I)	(3.0, 2.88, 11.5)	(3.0, 3.41, 13.6)	(3.0, 4.08, 16.3)	(3.0, 4.08, 16.3)
(II)	(0.0, 3.65, 11.5)	(0.0, 4.32, 13.6)	(0.0, 5.17, 16.3)	(0.0, 5.17, 16.3)

TABLE V. Averaged cross sections for the neutral-current (anti)neutrino scattering in units of 10^{-42} cm^2. The values on the left (right) correspond to computations with pairing strength G_n (G_p). Both pairing strengths give similar results for the scattering off ^{208}Pb. The results here are for the neutrino-parameter set (I). The full ranges of cross sections are produced by the consideration of the ranges of cross sections quoted in the other columns of this table.

	^{204}Pb			^{206}Pb		
Flavor	SkM*	SkX	SLy4	SkM*	SkX	SLy4
ν_e	5.86,6.30	8.99,9.23	5.62,5.91	5.75,6.07	9.40,9.60	5.68,5.96
$\bar{\nu}_e$	10.2,10.8	14.7,15.1	9.70,10.1	10.1,10.5	15.4,15.6	9.80,10.2
ν_x	22.5,23.5	30.8,31.4	21.2,21.9	22.4,23.1	32.1,32.5	21.5,22.1
$\bar{\nu}_x$	19.7,20.6	27.0,27.5	18.6,19.2	19.6,20.2	28.1,28.5	18.8,19.4

	^{208}Pb			Full range		
Flavor	SkM*	SkX	SLy4	^{204}Pb	^{206}Pb	^{208}Pb
ν_e	5.35	9.55	5.42	5.62–9.23	5.68–9.60	5.35–9.55
$\bar{\nu}_e$	9.60	15.7	9.55	9.70–15.1	9.80–15.6	9.55–15.7
ν_x	21.8	32.8	21.2	21.2–31.4	21.5–32.5	21.2–32.8
$\bar{\nu}_x$	19.0	28.6	18.5	18.6–27.5	18.8–28.5	18.5–28.6

$M1$ giant resonance, in accordance with the data, the total cross sections become the largest for the SkX interaction and thus also the averaged one. Furthermore, we give in Tables V and VI, in the "Full range" columns, ranges for cross sections from the smallest to the largest cross section predicted by the considered Skyrme interactions and pairing strengths. The full ranges show that the cross sections are practically independent of the Pb isotope for all neutrino flavors. Similar behavior is also observed for the charged-current reactions on Pb isotopes in [12].

In Fig. 5 we compare the calculated averaged cross sections with the results available in Ref. [31]. Our results have been obtained by using the quenching $(1/1.267)^2$. As seen from the figure, the averaged cross sections of Ref. [31] are between those of the SkX and SkM* interactions.

We visualize the contributions of various multipole channels to the averaged cross sections in the case of electron-neutrino scattering off ^{208}Pb in Fig. 6. We display the results obtained by using the SkX interaction, but the results for the other two interactions are similar. The averaged cross section is dominated by the 1^+ multipole channel with axial-vector nature. The same is true for the antineutrino reactions.

In Fig. 7 we show for the electron-neutrino scattering off ^{208}Pb the most prominent final states their multipolarity, excitation energies, and normalized differential cross sections to these states. The differential cross sections in the figure have been normalized by dividing the averaged differential cross sections by the total averaged cross section, i.e., all contributions of the excited states add up to 1. It can be seen in Fig. 7(a) that the transition to the 1^+_9 state at about 7 MeV dominates for the SkX interaction. The same is true for the other two nuclei. In the case of the SLy4 interaction [Fig. 7(c)] the transitions to the 1^+_{10} state at 9.7–9.9 MeV and to the 1^+_6 state at 7.5–7.6 MeV dominate for all nuclei. For the SkM* interaction the most prominent final states are 1^+_{10} at 10 MeV and 1^+_7 at 7.3 MeV in the ^{204,206}Pb nuclei and 1^+_{11} at 9.8 MeV and 1^+_6 at 7.2 MeV in the nucleus ^{208}Pb [see Fig. 7(b)]. It should be noted that these most prominent transitions correspond to

TABLE VI. Same as Table V, but for the neutrino-parameter set (II).

	^{204}Pb			^{206}Pb		
Flavor	SkM*	SkX	SLy4	SkM*	SkX	SLy4
ν_e	8.43,8.92	12.1,12.4	8.00,8.34	8.34,8.69	12.6,12.8	8.11,8.41
$\bar{\nu}_e$	13.8,14.5	19.1,19.4	13.1,13.5	13.7,14.2	19.8,20.1	13.2,13.6
ν_x	30.5,31.5	40.6,41.2	28.6,29.4	30.5,31.2	42.1,42.6	29.0,29.6
$\bar{\nu}_x$	25.9,26.8	34.5,35.0	24.4,25.1	25.8,26.4	35.7,36.1	24.6,25.2

	^{208}Pb			Full range		
Flavor	SkM*	SkX	SLy4	^{204}Pb	^{206}Pb	^{208}Pb
ν_e	7.95	12.8	7.87	8.00–12.4	8.11–12.8	7.87–12.8
$\bar{\nu}_e$	13.3	20.2	12.9	13.1–19.4	13.2–20.1	12.9–20.2
ν_x	29.9	43.0	28.7	28.6–41.2	29.0–42.6	28.7–43.0
$\bar{\nu}_x$	25.3	36.5	24.3	24.4–35.0	24.6–36.1	24.3–36.5

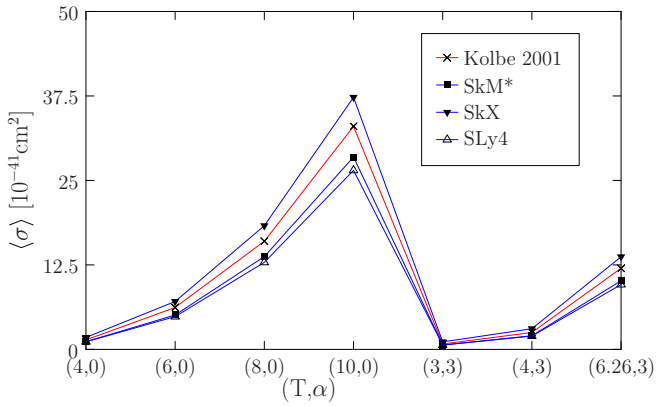

FIG. 5. Comparison between our averaged cross sections and those of Kolbe 2001 [31] for the neutrino scattering off ^{208}Pb. Our results are obtained by using the quenching factor $(1/1.267)^2$. The horizontal axis displays the (T, α) values used by [31].

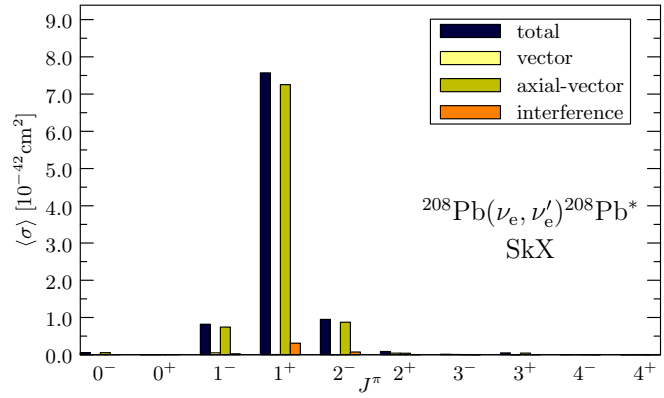

FIG. 6. Contributions of the different multipole channels to the averaged cross section of the electron-neutrino scattering off ^{208}Pb. The neutrino-parameter set (I) is used.

the transitions to the $M1$ giant resonance as clearly seen in Fig. 1. One can see that even the splitting of the the resonance is reproduced and the leading single-particle transitions are those quoted in connection with Fig. 1.

IV. CONCLUSIONS

This paper reports on the computed cross sections for the neutral-current neutrino and antineutrino scattering off the stable even lead isotopes. To our knowledge this is the first time that the NC scattering off the ^{204,206}Pb lead isotopes is discussed, in addition to the treatment of the scattering off ^{208}Pb. Our main focus is on (anti)neutrino scattering in the range of supernova-neutrino energies. The responses of the considered lead nuclei to supernova (anti)neutrinos are calculated by folding the cross sections with realistic energy profiles for the incoming (anti)neutrinos. The quasiparticle random-phase approximation (QRPA) is employed to

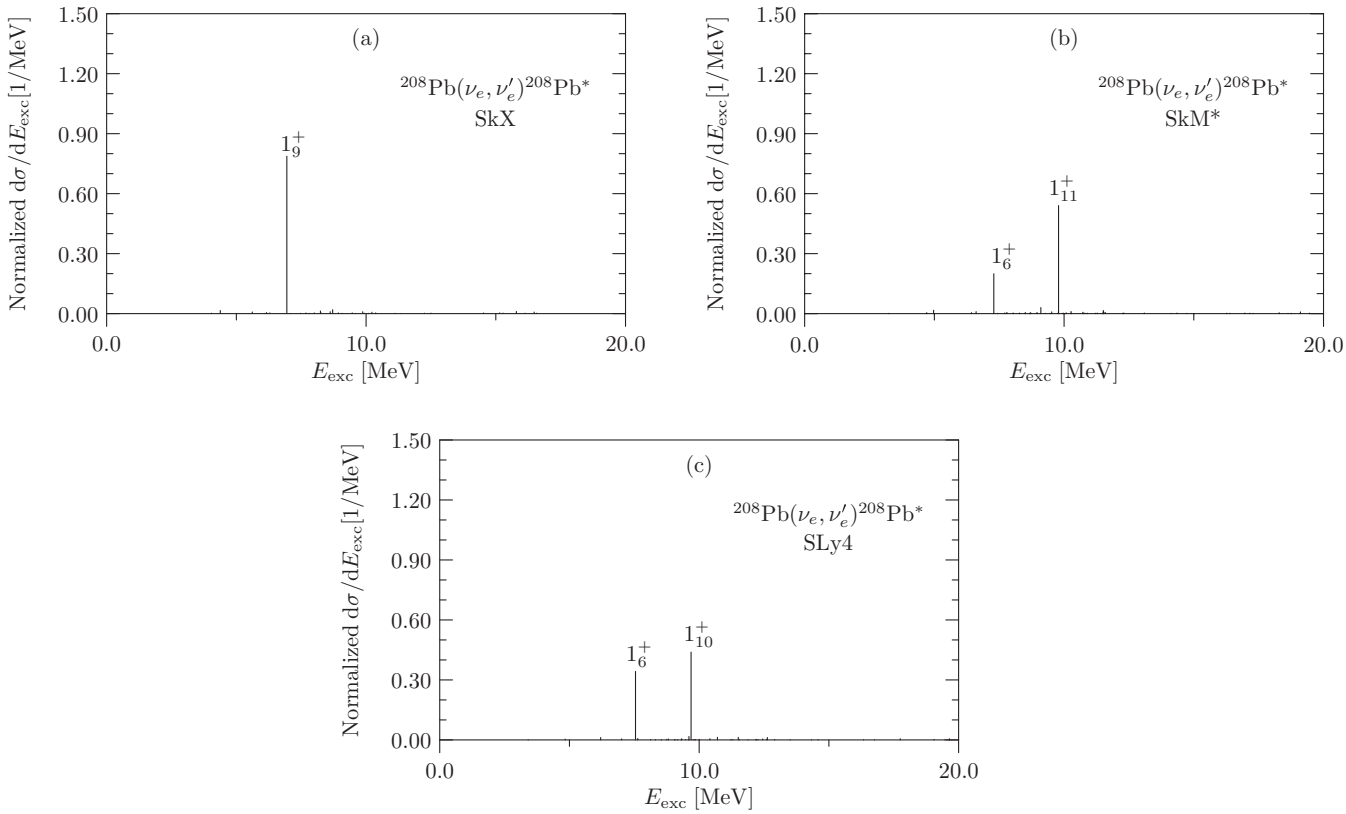

FIG. 7. Averaged differential cross sections for the electron-neutrino scattering off ^{208}Pb as functions of the excitation energy in the final nuclei. The result in (a) is obtained by using the SkX interaction, in (b) by using the SKM* interaction, and in (c) by using the SLy4 interaction.

construct the required nuclear wave functions of the scattering initial and final states. The two-body nucleon-nucleon forces used in this study are the Skyrme SkM*, SkX, and SLy4 interactions and they are applied both to form the quasiparticle mean field and the QRPA spectra, thus leading to a self-consistent evaluation of the nuclear excitations.

The strength distribution of the $M1$ transitions in ^{208}Pb is computed. The agreement with measurements is best for the SkX interaction, implying more reliable cross-section results for this interaction than for the other considered Skyrme interactions. This conclusion is based on the observations that for the neutral-current reactions the transitions mediated by the 1^+ multipole are the most important for the typical energies of supernova neutrinos and that the cross section is dominated by transitions to the $M1$ resonance state.

The total and averaged computed cross sections for ^{208}Pb were compared with the results available in the literature. These are based on several different nuclear-structure approaches. In general, a good agreement was found.

ACKNOWLEDGMENTS

This work was partially supported by the Academy of Finland under the Academy Project No. 318043. E.Y. is grateful for the financial support of the Grant No. 2016/25143-7 from the Sao Paulo Research Foundation (FAPESP).

[1] H. Ejiri, Phys. Rep. **338**, 265 (2000).
[2] J. Suhonen and O. Civitarese, Phys. Rep. **300**, 123 (1998).
[3] J. Maalampi and J. Suhonen, Adv. High Energy Phys. **2013**, 505874 (2013).
[4] J. Vergados, H. Ejiri, and F. Šimkovic, Int. J. Mod. Phys. E **25**, 1630007 (2016).
[5] H. Ejiri, J. Suhonen, and K. Zuber, Phys. Rep. **797**, 1 (2019).
[6] A. B. Balantekin and G. M. Fuller, J. Phys. G: Nucl. Part. Phys. **29**, 2513 (2003).
[7] K. Langanke and E. Kolbe, At. Data Nucl. Data Tables **79**, 293 (2001).
[8] J. H. Davis, J. Cosmol. Astropart. Phys. 03 (2015) 012.
[9] P. Pirinen, J. Suhonen, and E. Ydrefors, Adv. High Energy Phys. **2018**, 9163586 (2018).
[10] K. Scholberg, Annu. Rev. Nucl. Part. Sci. **62**, 81 (2012).
[11] Helium and Lead Observatory, http://www.snolab.ca/halo/.
[12] W. Almosly, B. G. Carlsson, J. Suhonen, J. Toivanen, and E. Ydrefors, Phys. Rev. C **94**, 044614 (2016).
[13] J. S. O'Connell, T. W. Donnelly, and J. D. Walecka, Phys. Rev. C **6**, 719 (1972).
[14] M. Bender, P.-H. Heenen, and P.-G. Reinhard, Rev. Mod. Phys. **75**, 121 (2003).
[15] B. A. Brown, Phys. Rev. C **58**, 220 (1998).
[16] H. Krivine, J. Treiner, and O. Bohigas, Nucl. Phys. A **336**, 155 (1980).
[17] J. Bartel, P. Quentin, M. Brack, C. Guet, and H. B. Håkansson, Nucl. Phys. A **386**, 79 (1982).
[18] E. Chabanat, P. Bonche, P. Haensel, J. Meyer, and R. Schaeffer, Nucl. Phys. A **635**, 231 (1998); **643**, 441(E) (1998).
[19] P. Vesely, J. Toivanen, B. G. Carlsson, J. Dobaczewski, N. Michel, and A. Pastore, Phys. Rev. C **86**, 024303 (2012).
[20] B. G. Carlsson, J. Toivanen, and A. Pastore, Phys. Rev. C **86**, 014307 (2012).
[21] B. G. Carlsson, J. Dobaczewski, J. Toivanen, and P. Vesely, Comput. Phys. Commun. **181**, 1641 (2010).
[22] E. Ydrefors, K. G. Balasi, J. Suhonen, and T. S. Kosmas, *Neutrinos: Properties, Reactions, Sources and Detection* (Nova Science, Hauppauge, NY, 2011).
[23] J. D. Walecka, *Theoretical Nuclear and Subnuclear Physics* (Imperial College, London, 2004).
[24] J. Suhonen, Front. Phys. **5**, 55 (2017).
[25] J. Kostensalo and J. Suhonen, Int. J. Mod. Phys. A **33**, 1843008 (2018).
[26] M. Dutra, O. Lourenco, J. S. Sá Martins, A. Delfino, J. R. Stone, and P. D. Stevenson, Phys. Rev. C **85**, 035201 (2012).
[27] W. Almosly, B. G. Carlsson, J. Dobaczewski, J. Suhonen, J. Toivanen, P. Vesely, and E. Ydrefors, Phys. Rev. C **89**, 024308 (2014).
[28] J. Birkhan, H. Matsubara, P. von Neumann-Cosel, N. Pietralla, V. Yu. Ponomarev, A. Richter, A. Tamii, and J. Wambach, Phys. Rev. C **93**, 041302 (2016).
[29] P. Vesely, J. Kvasil, V. O. Nesterenko, W. Kleinig, P.-G. Reinhard, and V. Yu. Ponomarev, Phys. Rev. C **80**, 031302(R) (2009).
[30] N. Auerbach and A. Klein, Phys. Rev. C **30**, 1032 (1984).
[31] E. Kolbe and K. Langanke, Phys. Rev. C **63**, 025802 (2001).
[32] J. Engel, G. C. McLaughlin, and C. Volpe, Phys. Rev. D **67**, 013005 (2003).
[33] O. Civitarese and T. Tarutina, Phys. Rev. C **94**, 054603 (2016).
[34] K. G. Balasi, E. Ydrefors, and T. S. Kosmas, Nucl. Phys. A **868-869**, 82 (2011).
[35] M. T. Keil and G. G. Raffelt, Astrophys. J. **590**, 971 (2003).